scientific reports

Check for updates

OPEN

Response of carbon storage to land use change and multi-scenario predictions in Zunyi, China

Yi Liu[1,2], Xuemeng Mei[1,2], Li Yue[1,2] & Mingming Zhang[1,2]✉

Evaluating and predicting how carbon storage (CS) is impacted by land use change can enable optimizing of future spatial layouts and coordinate land use and ecosystem services. This paper explores the changes in and driving factors of Zunyi CS from 2000 to 2020, predicts the changes in CS under different development scenarios, and determines the optimal development scenario. Woodland and farmland are the main land use types in Zunyi. Land use change was reflected mainly in the mutual conversion among woodland, farmland, and grassland and by their conversion to construction land and water. In 2000, 2010, and 2020, the CS in Zunyi was 658.77 × 10^6 t, 661.44 × 10^6 t, and 658.35 × 10^6 t, respectively. Woodland, farmland and grassland conversions to construction land and water were primarily responsible for CS loss. The normalized difference vegetation index (NDVI) is the main factor influencing the pattern of CS (q > 10%). Furthermore, the impacts of the human footprint index and population density are increasing. In 2030, the CS of Zunyi is trending downward. Under the ecological-farmland conservation scenario (ECS), the CS is estimated to be 656.67 × 10^6 t, with the smallest decrease (− 0.26%) among timepoints. The effective control of woodland and farmland weakens the trend of CS reduction.

Keywords Carbon storage, PLUS model, InVEST model, Driving factors, Zunyi

In recent years, the excessive emission of greenhouse gases has led to global warming and frequent extreme weather events, posing a serious threat to the stability of global ecosystems[1,2]. Terrestrial ecosystems absorb carbon through a series of biological processes and thus play crucial roles in the global carbon cycle and in mitigating climate change. They serve as vital components of the world's carbon sink function[2,3]. Vegetation and soil provide the primary sources of carbon, acting as the backbone of the global carbon cycle[4]. Many studies have shown that changes in land use types profoundly affect the carbon sequestration capacity of terrestrial ecosystems, serving as a direct driving factor behind variations in CS[5]. In the past, rapid industrial development and urbanization in China have led to significant changes in land use patterns, as large areas of farmland and natural ecological land have been converted into artificial land. This process has resulted in noticeable carbon loss and has had a significant negative impact on the stability of China's ecosystems[4,6]. As the world's largest carbon emitter[7], China has set an ambitious goal to peak its carbon emissions by 2030 and achieve carbon neutrality by 2060[8,9]. Therefore, exploring the response of terrestrial ecosystem CS to land use change and analyzing the deep-seated driving factors affecting spatial heterogeneity are of paramount importance. These studies are crucial for enhancing terrestrial ecosystem carbon sequestration and maintaining the balance and stability of ecosystems.

Research on CS usually requires coupling multiple models for current situation analysis and future prediction. The Integrated Valuation of Ecosystem Services and Tradeoffs (InVEST) model is widely used in current terrestrial ecosystem CS assessments[10–12]. Compared with traditional methods such as the Intergovernmental Panel on Climate Change (IPCC) inventory method[13,14] and the atmospheric inversion method[15], the InVEST model offers advantages such as parameter flexibility, high precision, and high efficiency. Furthermore, remote sensing technology can be combined with it to visually represent and reflect spatial distributions. This approach facilitates further analysis of the spatiotemporal evolution characteristics of CS and its response to land use changes[16]. In addition, many current studies have combined the InVEST model with predictive models such as CLUE[17], FLUS[18,19], and CA-Markov[20] to evaluate changes in land use patterns and ecosystem CS under future scenarios based on analyses of historical evolutionary patterns and the driving factors of CS. The patch-generating land use simulation (PLUS) model, through the land expansion analysis strategy (LEAS) and the cellular automata (CA) model, better captures the principles and patterns of various land use changes[21]. This model can simulate the changes in various land use patches during the research phase and accurately predict land

[1]College of Forestry, Guizhou University, Guiyang 550025, Guizhou, China. [2]Research Center for Biodiversity and Nature Conservation, Guizhou University, Guiyang, China. ✉email: mmzhang@gzu.edu.cn

use change patterns under different policy scenarios. Therefore, under scenarios of intensified land succession in the future, the PLUS model can more accurately simulate future land use development[22].

Zunyi is located in the Wujiang River Basin in the upper reaches of the Yangtze River. It plays a crucial role in strengthening the ecological barrier in the upper reaches of the Yangtze River. Zunyi is also a karst limestone distribution area in Southwest China[23]. The karst ecosystem in this region is characterized by low environmental carrying capacity, high sensitivity, and poor stability[24]. In recent years, with the continuous development of population growth and urbanization, land use changes have become relatively drastic, and the ecosystem balance in this region is facing great challenges[23]. Therefore, this study coupled the PLUS, InVEST, and optimal parameter geographic detector (OPGD) models to design a comprehensive research framework for evaluating CS under different future scenarios. The objectives of this study are as follows: (1) reveal the spatiotemporal changes in land use types and their responses to carbon storage; (2) identify the main driving factors and mechanisms influencing the CS patterns in Zunyi; and (3) predict CS changes under various development scenarios and determine the optimal development model. The findings of this study provide a reference for enhancing the ecosystem carbon sequestration capacity of Zunyi, optimizing ecological protection policies, reinforcing the ecological barrier in the upper reaches of the Yangtze River, and achieving green and sustainable economic development.

Materials and methods

Study area

Zunyi (105°36′–108°13′E, 27°8′–29°12′N) is located in the northern part of Guizhou Province and is situated in the transitional slope zone that stretches from the Yunnan–Guizhou Plateau to the Hunan Hills and the Sichuan Basin (Fig. 1). The area features complex topography and is part of the ecological barrier in the upper reaches of the Yangtze River, where it plays a crucial role in the ecological stability of Guizhou Province and even the Yangtze River Basin (data sourced from the Zunyi Municipal Government website, https://www.zunyi.gov.cn/). The terrain within Zunyi is diverse and consists primarily of basins and hills, ranging from 1000 to 1600 m in elevation. It has a subtropical humid monsoon climate; its vegetation is predominantly subtropical evergreen broad-leaved forests. Zunyi is also a biodiversity hotspot in Guizhou Province, and its unique topography and climate provide a sanctuary for numerous rare and endangered species, such as *Trachypithecus francoisi* and *Cathaya argyrophylla Chun & Kuang*[25]. Zunyi has established nature reserves covering an area of 294,600 hm^2, accounting for 9.57% of the total land area. These reserves form a relatively complete system of

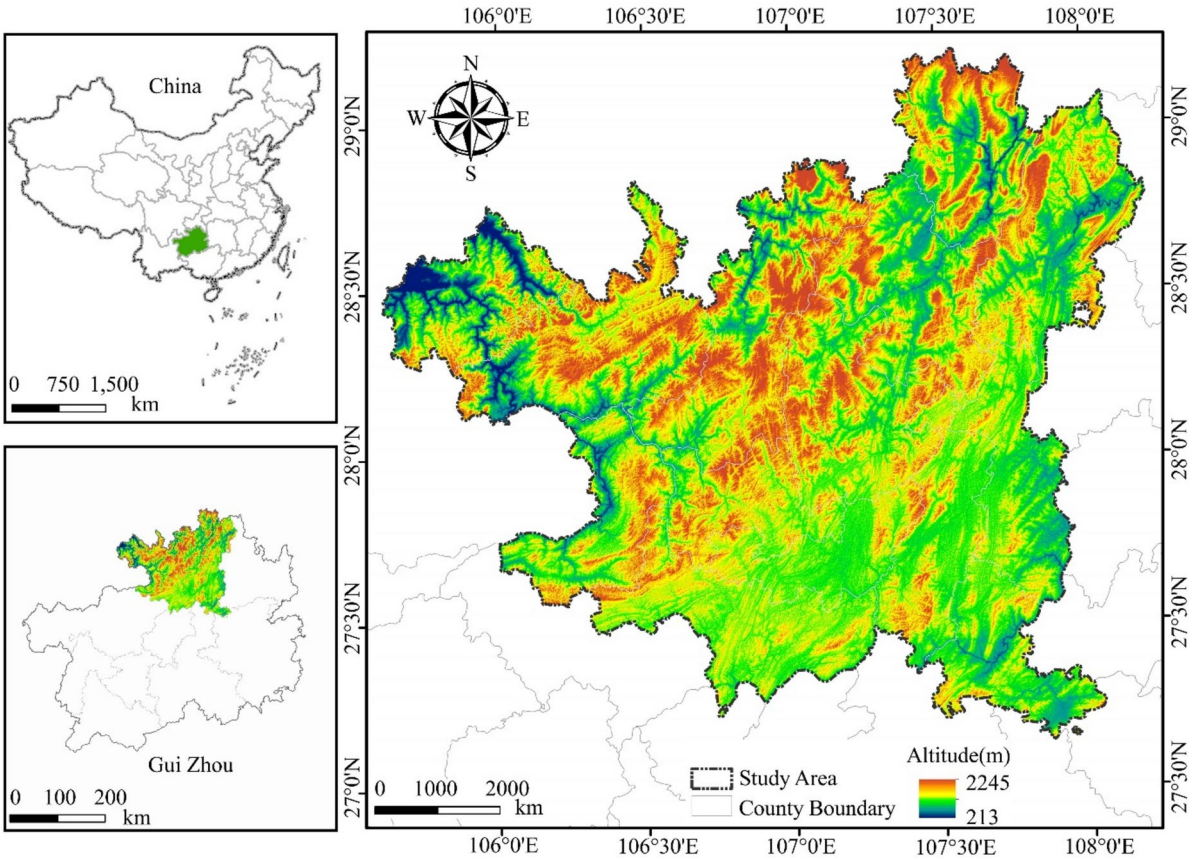

Fig. 1. Study area. This map was created via ArcGIS 10.8 (http://www.esri.com/). The administrative division data of China in the map come from the Data Center for Resources and Environmental Sciences, Chinese Academy of Sciences. (https://www.resdc.cn/).

natural protected areas. This is highly important for the ecological protection strategy of Guizhou Province[26]. Zunyi has a high forest coverage rate, but the karst landscape dominated by carbonate rocks results in a relatively fragile ecosystem[23]. In recent years, with the rapid development of the wine industry and urbanization, land use changes have been drastic, as the demand for construction land has increased. This situation has created a stark conflict between urban development and ecological protection, significantly challenging the ecosystem's carbon sequestration capacity.

Data sources

The basic land use datasets (2000, 2010 and 2020) used in this study were sourced from the Data Center for Resources and Environmental Sciences, Chinese Academy of Sciences (https://www.resdc.cn/), which are based on Landsat remote sensing image data interpretation. According to the land resources and their utilization attributes, the data were divided into 6 categories: farmland (land used for growing crops, including paddy fields and dry fields), woodland (forestry land where trees, shrubs, bamboo, and coastal mangroves grow), grassland (various types of land dominated by herbaceous plants, with coverage of over 5%), water (natural terrestrial water bodies and land used for water conservancy facilities), construction land (land used for urban and rural residential areas, as well as industrial, mining, and transportation purposes) and unused land (land that is currently unused, including land that is difficult to utilize, such as sandy land, gobi, saline-alkali land, marshland, bare land, and exposed rocky areas), with a spatial resolution of 30 m. Other data sources for PLUS simulation and driver exploration are shown in Table 1.

Methods

The research framework, as shown in Fig. 2, comprises three main components. The PLUS model was used to predict the spatial patterns of land use and CS under different scenarios. The InVEST model was used to evaluate the spatiotemporal characteristics of the ecosystem CS in Zunyi, and the impact of land use changes on the carbon sequestration capacity was explored. The OPGD model was used to analyze the driving factors influencing ecosystem CS.

PLUS model

The PLUS model is suitable for accurately simulating future land use development in scenarios where land selection intensifies in the future. The PLUS model is suitable for accurately simulating future land use development in the case of intensified land separation. The model includes two modules: the land expansion analysis strategy (LEAS) and the CA model, which is based on many random patch seeds (CARSs)[22,27].

LEAS

It employs the random forest algorithm to analyze the relationships between various driving factors and the expansion of different land use types, with the aim of assessing the development probability of future land

Type	Data	Data usage	Type/resolution	Data resource
Basic data	Administrative boundary	–	shp	https://www.resdc.cn/
	Land use datasets (2000\2010\2020)	Land use change and PLUS	tif/30 m	https://www.resdc.cn/
	Protected area vector data in Zunyi	PLUS-Restricted area	shp	https://zrzy.guizhou.gov.cn/
Climatic and topographic data	DEM	PLUS and OPGD(X1)	tif/30 m	https://www.gscloud.cn/
	Slope	PLUS and OPGD(X2)	tif/30 m	
	Aspect of slope	PLUS	tif/30 m	
	Annual average temperature	PLUS and OPGD(X3)	tif/1000 m	https://www.resdc.cn/
	Annual average precipitation	PLUS and OPGD(X4)	tif/1000 m	
	NDVI	PLUS and OPGD(X5)	tif/30 m	
	Soil type	PLUS		
Socioeconomic data	Night-time light index	PLUS and OPGD(X6)	tif/1000 m	https://dataverse.harvard.edu/dataset.xhtml?persistentId=doi:10.7910/DVN/GIYGJU
	Human footprint index	PLUS and OPGD(X7)	tif/1000 m	https://doi.org/10.1038/s41597-022-01284-8
	GDP	PLUS and OPGD(X8)	tif/1000 m	https://www.resdc.cn/
	Population density	PLUS and OPGD(X9)	tif/1000 m	
	Proximity to water	PLUS	tif/30 m	https://www.webmap.cn/
	Proximity to railway	PLUS	tif/30 m	
	Proximity to highway	PLUS	tif/30 m	
	Proximity to primary road	PLUS	tif/30 m	
	Proximity to secondary road	PLUS	tif/30 m	
	Proximity to tertiary road	PLUS	tif/30 m	
	Proximity to country road	PLUS	tif/30 m	
	Proximity to government seat	PLUS	tif/30 m	

Table 1. Data sources.

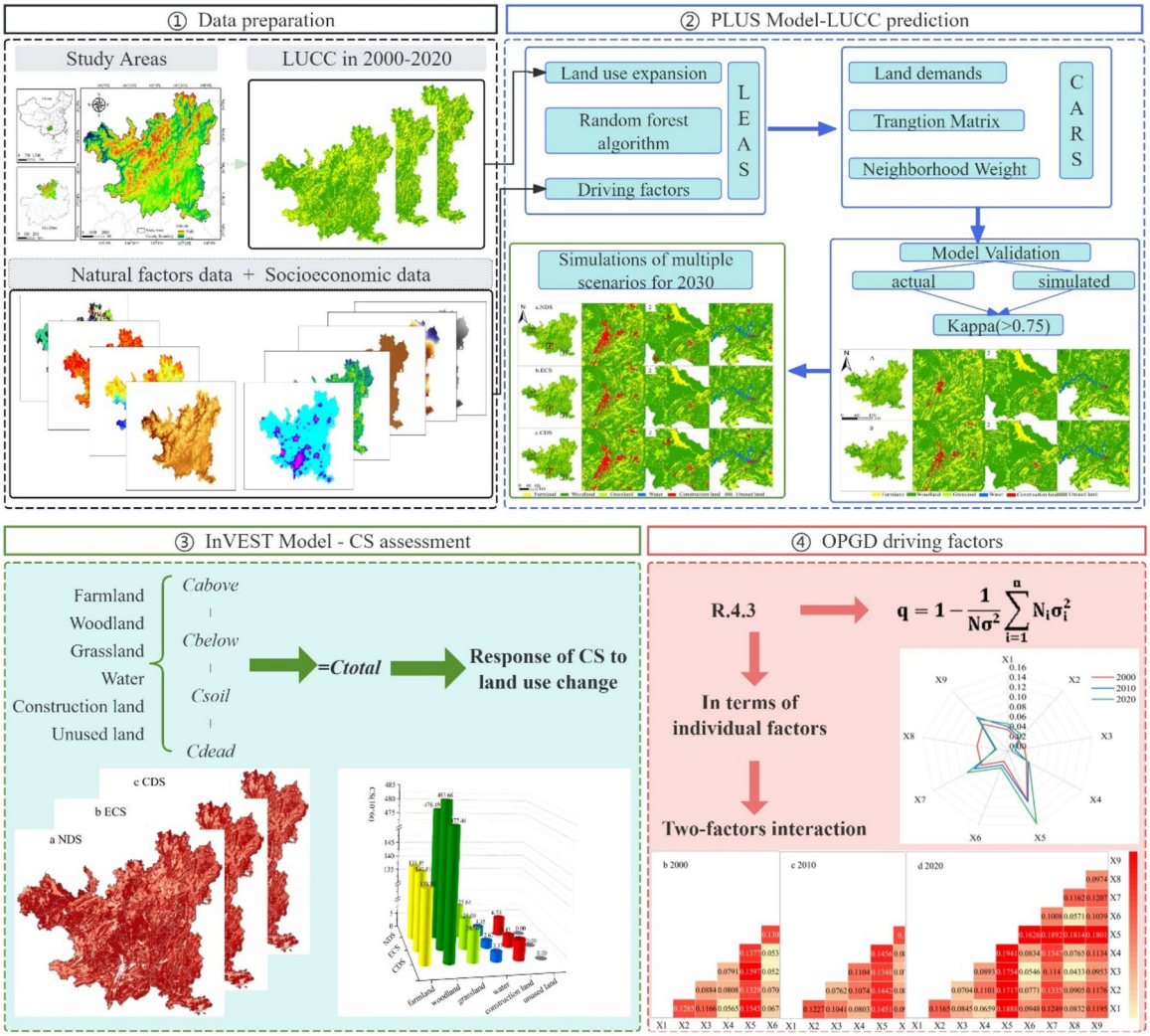

Fig. 2. The research framework (created by the Adobe Photoshop 2020, https://www.adobe.com/).

use types. For this analysis, we selected 19 factors based on environmental, geographical, and socioeconomic elements. Using land use data from 2000, 2010, and 2020, we predicted the development probabilities of different land use types in Zunyi.

CARS

This module integrates the generation of random patch seeds to simulate future land use patterns. During this process, we did not restrict the land use transfer cost matrix; instead, we designed different probabilities for land use type transitions based on various scenarios. The probability of random patch seeding was set as 0.1, and the neighborhood factors of farmland, woodland, grassland, water, construction land and unused land were set as 0.49, 0.98, 0.62, 0.21, 0.66, and 0.01, respectively, and its range was 0–1 (the closer to 1, the higher the expansion capacity of the land use type).

Model accuracy verification

To ensure that the model can be used for future land use simulation predictions in the study area, 2020 land use data were simulated and compared with actual land use data for validation. The results revealed that the kappa coefficient was 0.84, and the overall accuracy was 0.90 (Fig. 3). The results show high simulation accuracy, indicating its feasibility for predicting land use changes in 2030.

Simulations of multiple scenarios for 2030

We fully integrated the population growth and urbanization development trends in Zunyi, determined the historical development patterns of land use types, and referred to relevant data from the overall land spatial planning of Guizhou Province (https://zrzy.guizhou.gov.cn/) and Zunyi (https://zrzyj.zunyi.gov.cn/). According to relevant documents, Zunyi will strengthen the core status of the central urban area while strictly controlling the "three control lines" to effectively protect farmland, adhere to the bottom line of ecological security, and

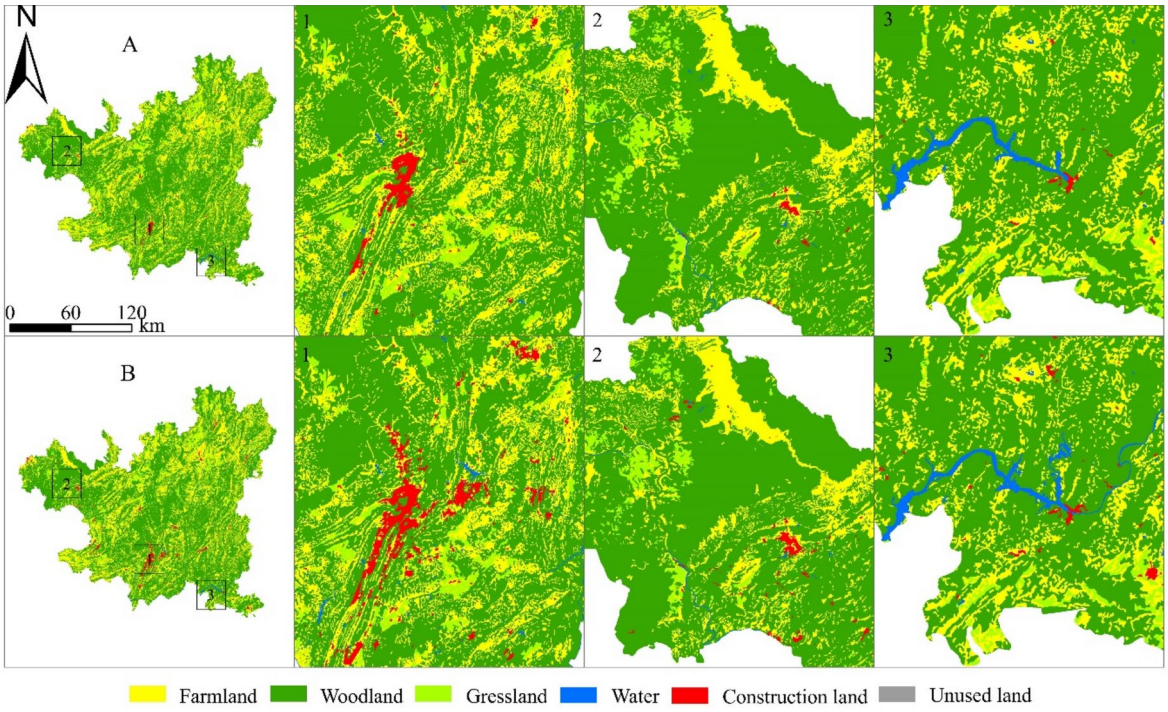

Fig. 3. Comparison of land use simulation results (**A**) and actual data (**B**) from ZunYi for 2020 (created by ArcGIS 10.8, http://www.esri.com/).

improve the construction of the natural protected area system. Therefore, the following three scenarios are used to simulate the land use situation in 2030:

Natural development (NDS)
Based on the land use pattern of 2020 and without considering other interfering factors, the conversion rate of land use types has remained unchanged over time.

Ecological-farmland conservation (ECS)
Farmlands and woodlands are directly related to national food security and ecological security. The protection of ecology and farmland will be prioritized in future social development, thereby promoting high-quality economic development. Therefore, in the ECS scenario, the natural reserves, reservoirs, and river basins are used as restriction areas, thus decreasing the probability of woodland and farmland conversion to construction land by 40% while decreasing the probability of conversion to grassland by 30%. Moreover, the probability of grassland conversion to woodland will increase by 30%, and the probability of conversion to construction land will decrease by 20%.

Urban development (CDS)
The scenario assumes that the region experiences rapid economic development, leading to the expansion of construction land. The probability of woodland, forestland, and grassland conversion into construction land increases by 20%, and the probability of unused land conversion into construction land increases by 30%. The probability of construction land conversion into grassland, woodland, and water decreased by 50%.

InVEST-CS module

The InVEST model has strong spatial analysis capabilities and enables the visualization of dynamic ecosystem service functions. The carbon storage and sequestration module of InVEST 3.14.0 divides CS into four basic carbon pools: above carbon, below carbon, soil carbon, and dead organic carbon. The CS of the ecosystem is calculated as follows:

$$C_{total} = C_{above} + C_{below} + C_{soil} + C_{dead} \quad (1)$$

where C_{total} is the total carbon density (t·hm^{-2}), C_{above} is the aboveground carbon density of living plants, C_{below} is the belowground carbon density of living plants, C_{soil} is the soil carbon density, and C_{dead} is the dead organic carbon density.

Land use type	C_{above}	C_{below}	C_{soil}	C_{dead}
Farmland	36.48	6.93	109.68	1.02
Woodland	58.27	17.50	173.40	3.50
Grassland	1.32	1.40	135.00	1.00
Water	2.75	0.00	112.50	0.00
Construction land	0.00	0.00	108.50	0.00
Unused land	0.74	0.13	69.92	0.00

Table 2. Carbon density table of land use types (t·hm^{-2}).

Judgment basis	Interaction types
q (X1∩X2) < min[q(X1), q(X2)]	Nonlinear strengthening weakened
min[q(X1), q(X2)] < q (X1∩X2) < max[q(X1), q(X2)]	Single factor nonlinear weakening
q (X1∩X2) > max[q(X1), q(X2)]	Two-factor enhancement
q(X1∩X2) = q(X1) + q(X2)	Independence
q(X1∩X2) > q(X1) + q(X2)	Nonlinear enhancement

Table 3. Types of two-factor interactions with the CS.

To obtain accurate carbon density values for various land use types, we referenced empirical carbon density data from studies conducted in Zunyi and its surrounding areas[28–30]. Additionally, we applied a correction formula for carbon density proposed by Alam et al.[31–33], and the correction was combined with the precipitation factor.

$$C_{BP} = e^{0.0054 \times MAP} \times 6.798 \tag{2}$$

$$C_{SP} = 3.3958 \times MAP + 1996.1 \tag{3}$$

$$K_{BP} = \frac{C_{BP}^{1}}{C_{BP}^{2}} \tag{4}$$

$$K_{SP} = \frac{C_{SP}^{1}}{C_{SP}^{2}} \tag{5}$$

where C_{BP} is the corrected biomass carbon density; C_{SP} is the corrected soil carbon density; MAP is the mean annual precipitation; K_{BP} is the correction for the biomass carbon density precipitation factor; and K_{SP} is the correction for the soil carbon density precipitation factor. The final corrected carbon density data for various land use types are shown in Table 2.

OPGD model

Geographic detector models can explore the impact mechanism of different potential factors from single-factor and two-factor combinations and are widely used in the field of ecological environment research[34,35]. The OPGD model based on R4.3 automatically selects the optimal spatial discretization method to handle continuous variables, thus overcoming the subjectivity of manual discretization[36] and significantly improving the accuracy and applicability of factor detection results[37,38]. Therefore, in this study, the OPGD model was used to investigate the driving factors in different periods. Based on the availability of data and previous relevant studies, we selected 9 factors from the perspective of natural and socioeconomic data, including DEM (X1), slope (X2), annual average precipitation (X3), annual average temperature (X4), NDVI (X5), nighttime light index (X6), human footprint index (X7), GDP (X8), and population density (X9). With the assistance of ArcGIS 10.8 software, 1389 sample points were randomly sampled within the study area (with a threshold of 2000 m), and variable data were extracted. The impacts of the individual environmental factor q (X1) and the combined factor q (X1∩X2) on the spatial distribution of ecosystem CS were analyzed (Table 3). The formula for calculating the q value is as follows:

$$q = 1 - \frac{1}{N\sigma^2} \sum_{i=1}^{n} N_i \sigma_i^2 \tag{6}$$

where N_i and N are the numbers of cells in region i and the whole region, respectively; and σ_i^2 and σ^2 are the variances in region i and the entire region, respectively. n is the number of regions. The value of q ranges from 0 to 1, indicating the degree to which the driving factor explains the CS in the region. A q value closer to 1 indicates a greater impact on the differentiation of CS in the region, and vice versa.

Hot-spot analysis (Getis-Ord Gi*)

Hotspot analysis can reveal the spatial clustering patterns of high and low CS values within a certain spatial range[39]. This study aims to characterize the regional carbon sequestration capacity by using the changes in CS from 2000 to 2020 to identify hot spots and cold spots related to the carbon sequestration capacity.

First, global Moran's I was used to conduct spatial autocorrelation analysis[40]. When the value is between −1 and 1, a positive correlation is realized when it is > 0, and the closer the value is to 1, the greater the clustering effects of CS. The formula for calculating the global Moran's I index is as follows:

$$Q = \frac{n\sum_{i=1}^{n}\sum_{j=1}^{n}\omega_{ij}\left(x_i-\overline{x}\right)\left(x_j-\overline{x}\right)}{\sum_{i-i}^{n}\left(x_i-\overline{x}\right)^2} \tag{7}$$

$$Z_{score} = \frac{I-E\left(Q\right)}{\sqrt{VAR\left(Q\right)}} \tag{8}$$

where Q is the global Moran's I index; n is the total number of regions; x_i and x_j are the CSs of region i and region j, respectively; $\overline{x}$ is the average CS; n is the total number of study units; ω_{ij} is the spatial weight coefficient matrix of region i to region j; and $E(Q)$ and $VAR(Q)$ are the expected value and variance of the global Moran's I index x, respectively.

Second, using the hot-spot analysis tool, which is based on a grid scale of 1000 m × 1000 m, the aggregation phenomenon of CS in Zunyi was detected, and the carbon sequestration capacity hotspots were identified. The calculation formula is as follows:

$$G_i^* = \frac{\sum_{j=1}^{n} w_{ij}x_j - \overline{x}\sum_{j=1}^{n} w_{ij}}{S\sqrt{\frac{\left[n\sum_{j=1}^{n} w_{ij}^2 - \left(\sum_{j=1}^{n} w_{ij}\right)\right]^2}{n=1}}} \tag{9}$$

where w_{ij} is the spatial weight matrix of grid i and grid j; and x_j is the CS of grid j, where $\overline{x}$ is the average CS, S is the standard deviation of the CS, and n is the total number of grids.

Results

Spatiotemporal evolution of land use and CS from 2000–2020

Characteristics of the land use changes

The main land use types in Zunyi are woodland and farmland. Woodlands are widely distributed in the study area (> 62%) and are concentrated in the northwest and middle parts. Additionally, it highly overlaps with protected areas. The farmland area accounts for approximately 30% of the total area, which is fragmented and dispersed. The construction land is concentrated in southern China and southwest China, with a noticeable expansion trend (Fig. 4a,b). Other types of land are sporadically distributed. From 2000 to 2020, areas involving various types of land use underwent varying degrees of change. Woodlands experienced significant fluctuations from 2000 to 2020, with a total increase of 10,623.42 hm^2 and a proportional increase of 0.35%. It increased by 26,279.91 hm^2 (+0.86%) from 2000 to 2010, followed by a decrease of 15,656.49 hm^2 (−0.51%) from 2010 to

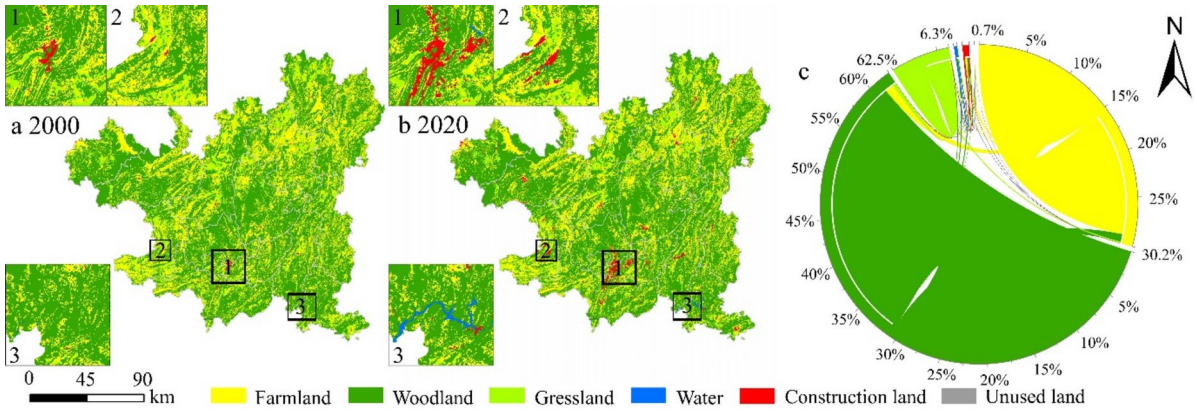

Fig. 4. (**a**,**b**) Land use pattern. (**c**) String map of land use transfer from 2000 to 2020 (created by ArcGIS 10.8, http://www.esri.com/).

2020. Farmland and grassland decreased by 28,371.87 hm^2 and 23,398.2 hm^2, respectively, representing decreases of 0.92% and 0.76%, respectively, indicating a continuous downward trend. Construction land experienced significant outward expansion, increasing from 0.25 to 1.17%, with an increase of 28,160.82 hm^2. Concurrently, the water area grew by 12,996.99 hm^2.

From 2000 to 2020, Zunyi experienced a total land use change of 204,073.02 hm^2, characterized by the mutual conversions among woodland, farmland, and grassland and by their conversions to construction land and water (Fig. 4c). Farmland experienced a net outflow of 28,372.05 hm^2, which was converted primarily to construction land (17,017.11 hm^2). Grassland experienced a net outflow of 23,398.2 hm^2 and was converted mainly to woodland (23,486.31 hm^2) and cropland (10,328.31 hm^2). Construction land significantly expanded, with a net inflow of 28,160.82 hm^2, sourced mainly from the conversion of farmland (17,017.11 hm^2) and woodland (9,443.52 hm^2). There was also a net inflow of 12,996.9 hm^2 of water, primarily from the conversion of woodland (8,546.76 hm^2) and farmland (4,150.62 hm^2).

Spatial–temporal distribution of CS

The total CS in Zunyi in 2000, 2010 and 2020 was 658.77 × 10^6 t, 661.44 × 10^6 t and 658.35 × 10^6 t, respectively. Compared with that in 2000, the total CS in 2020 decreased by 0.42 × 10^6 t, a decrease of 0.06%. During the study period, the total CS initially increased but then decreased. In 2010, the total CS increased by 2.67 × 10^6 t compared with that in 2000, an increase of 0.4%; however, in 2020, it decreased by 3.08 × 10^6 t compared with that in 2010, a decrease of 0.47%.

The average grid-based CS levels were 19.29 t/hm2, 19.36 t/hm2, and 19.27 t/hm2 for 2000, 2010, and 2020, respectively. Spatially, the high-value CS area was distributed mainly in the western and central areas of woodland concentration, whereas the low-value CS areas, such as the main urban area and Renhuai, were found where construction land was concentrated. In addition, the construction of artificial lakes in the southeastern region transformed part of the woodland into water, resulting in areas with low-value CS (Fig. 5).

Response of CS to land use change

First, we used the Kendall coefficient to test the correlation between land use change and CS variation. The results indicate a significant negative correlation between land use change and CS (−0.298, P = 0.0000). Woodland and farmland contributed to more than 90% of the total CS in Zunyi (Table 4). From 2000 to 2010, the increase in CS came mainly from woodland expansion, which contributed to 6.64 × 10^6 t of CS growth and thus compensated for the decrease in CS caused by reductions in farmland and grassland areas. From 2010 to 2020, the common

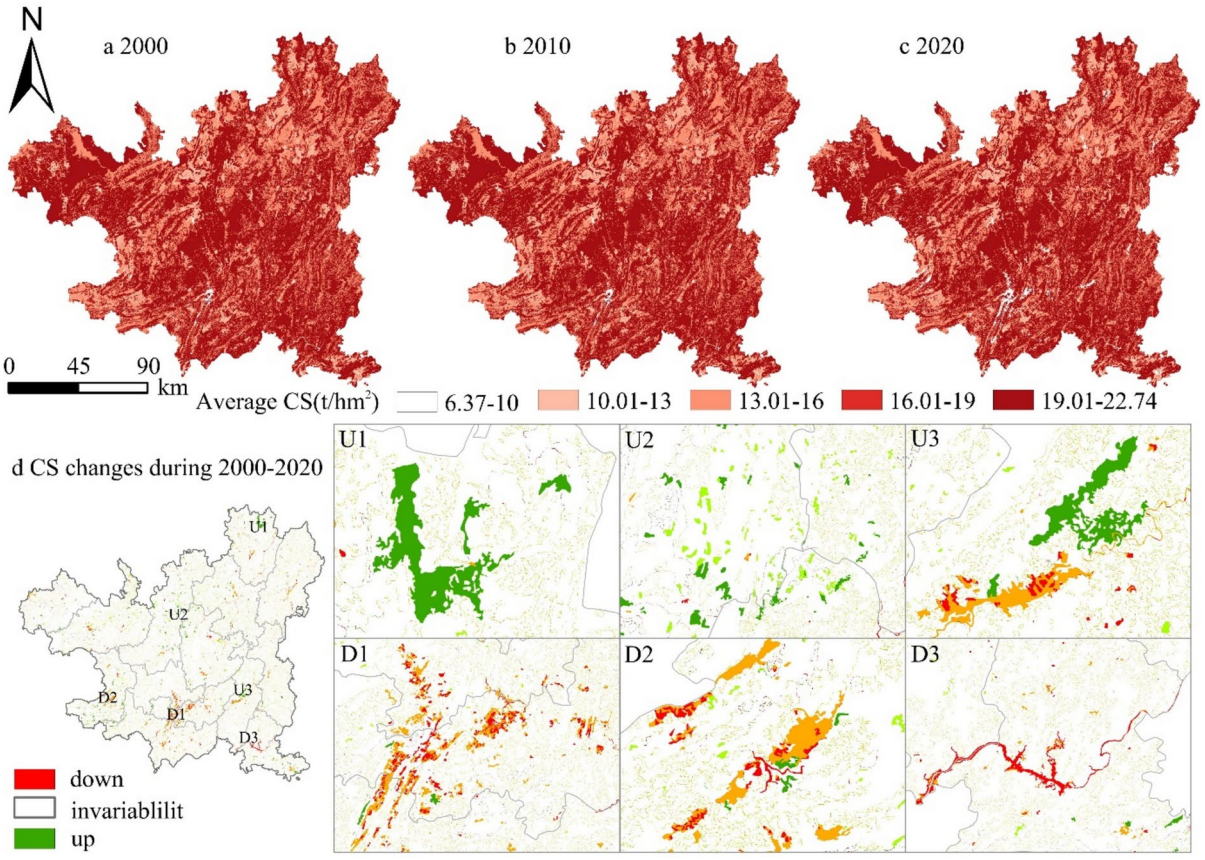

Fig. 5. (**a**,**b**,**c**) Distribution of CS in ZunYi. d. Distribution of CS changes (created by ArcGIS 10.8, http://www.esri.com/).

Type		2000	2010	2020
Farmland	area(hm^2)	941,317.29	930,905.19	912,945.42
	CS (10^6 t)	145.05	143.44	140.68
Woodland	area(hm^2)	1,915,771.77	1,942,051.68	1,926,395.19
	CS (10^6 t)	484.06	490.70	486.74
Grassland	area(hm^2)	203,814.81	182,065.05	180,416.61
	CS (10^6 t)	28.27	25.26	25.03
Water	area(hm^2)	4905.54	7154.91	17,902.53
	CS (10^6 t)	0.55	0.80	2.01
Construction land	area(hm^2)	7690.05	11,348.19	35,850.87
	CS (10^6 t)	0.83	1.23	3.89
Unused land	area(hm^2)	57.60	32.31	46.71
	CS (10^6 t)	0.00	0.00	0.00

Table 4. CS contributions by land use type (2000–2020).

	2020						
2000	Farmland	Woodland	Grassland	Water	Construction land	Unused land	Total
Farmland	0.00	6,081,557.27	− 128,734.03	− 172,624.25	− 775,809.83	− 67.47	5,004,321.69
Woodland	− 5,131,894.52	0.00	− 563,796.21	− 1,197,999.46	− 1,361,472.36	− 2799.13	− 8,257,961.68
Grassland	158,746.10	2,676,265.48	0.00	− 21,455.30	− 64,831.85	− 73.36	2,748,651.08
Water	7549.83	41,643.11	861.33	0.00	− 123.12	0.00	49,931.15
Construction land	12,444.70	22,797.60	712.59	84.96	0.00	0.00	36,039.85
Unused land	1896.74	343.75	85.59	93.85	0.00	0.00	2419.93
Total	− 4,951,257.15	8,822,607.22	− 690,870.73	− 1,391,900.19	− 2,202,237.16	− 2939.97	− 416,597.99

Table 5. CS change due to land use transfer (t).

reduction in farmland, woodland and grassland areas led to the loss of 6.95 × 10^6 t of CS; this decrease was primarily responsible for the decrease in total CS during this period. Construction land and water expanded significantly; however, owing to their low carbon density, their expansion could not compensate for the overall decline in CS.

Among the changes in CS caused by land use transfer, from 2000 to 2010, the transfer of land use resulted in a net increase of 2.67 × 10^6 t of CS, which was due mainly to the expansion of woodland. The transfer of farmland and grassland to woodland resulted in a net increase of 5.21 × 10^6 t of CS, but the transfer of woodland to farmland, construction land and water also caused a loss of 2.25 × 10^6 t of CS. From 2010 to 2020, land use transfer caused a net loss of 3.08 × 10^6 t of CS, which was due mainly to the transfer of woodland and farmland. The transfer of both construction land and water resulted in a total loss of 2.96 × 10^6 t of CS. In general, the change in CS in the study area is strongly affected by changes in woodlands and farmlands (Table 5). When farmland and woodland areas with relatively high carbon densities are transferred or construction land is significantly expanded, many CS losses occur[16,41].

CS hot spots from 2000 to 2020

The global Moran's I indices of CS in 2000, 2010 and 2020 were 0.6168, 0.6115 and 0.6009, respectively (P = 0.0000), indicating that the spatial aggregation effect of CS in Zunyi was significant but gradually weakened.

The Getis–Ord G*i analysis results revealed that the hot spots of CS in all of Zunyi were clustered in the western and central regions but gradually decreased over the study period. In contrast, the cold spots of CS were relatively dispersed and exhibited a certain degree of expansion (Fig. 6a,b). On a temporal scale, the change in CS in Zunyi from 2000–2020 was analyzed to characterize the carbon sequestration capacity (Fig. 6c). The results revealed that the number of hot spots for carbon sequestration was less than the number of cold spots. Carbon sequestration hotspots were distributed in the northern part of Zunyi. The vector boundaries of the natural reserves were overlaid, and the results revealed that the majority of the hot spots were distributed in natural reserves and adjacent areas. This finding indicates that the policy constraints of natural reserves restricted the outflow of woodland and, to some extent, positively drove changes in adjacent areas by promoting the transformation of land from protected areas and surrounding areas into woodland, thus improving the carbon sequestration capacity. Carbon sequestration cold spots were concentrated in the southern and western parts of the country. Additionally, there were cold spots in Yuqing in the southeastern part, mainly due to the transformation of woodland into water.

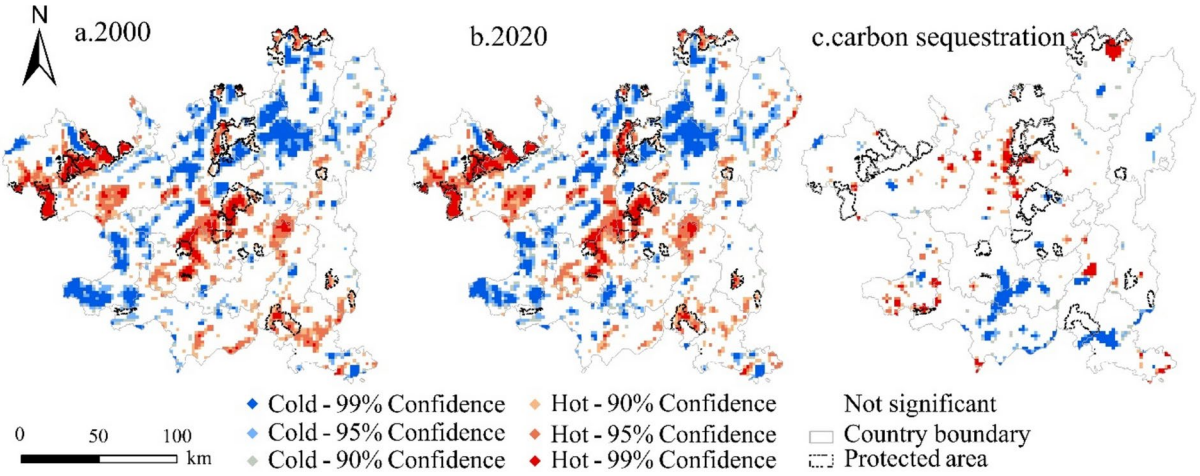

Fig. 6. (**a**,**b**) Carbon density hot/cold spots. (**c**) Distribution of carbon sequestration hot/cold spots from 2000 to 2020 (created by ArcGIS 10.8, http://www.esri.com/).

Driving factors of the spatiotemporal pattern of CS

The factor detection results revealed that both natural and human factors have significant impacts on the spatial distribution of CS in Zunyi, but the influence of each driving factor varies across different periods. In terms of individual factors, NDVI(X5) > population density(X9) > human footprint index(X7) > DEM(X1) > annual average temperature(X4); the other factors have relatively low explanatory power. The explanatory power of X5 (0.11, 0.11, 0.16, p = 0.00) exceeded 10% during the study period, which was the main factor driving the spatial pattern of CS in Zunyi. Additionally, the explanatory power of the human footprint index (X7) and population density (X9) continuously increased.

The interaction detection results show that each driving factor exhibits nonlinear enhancement or two-factor enhancement, indicating that the combined effects of various factors have a greater impact on the spatial pattern of CS. In 2000, the types of synergy that had the greatest impact on the spatial pattern of CS were GDP and NDVI, with q values of 0.16. In 2010, the greatest impact was from the synergy between population density and the NDVI, with an interaction detection q value of 0.15. In 2020, the greatest impact was from the synergy between the annual average temperature and the NDVI, with an interaction detection q value of 0.19 (Fig. 7b–d). The synergies between the NDVI and GDP, population density, and annual average temperature exhibited significant nonlinear enhancements, greatly influencing the spatial distribution pattern of CS.

Multiscenario simulation forecast for 2030

2030 Land use pattern

Under the NDS, the area of construction land in Zunyi increases the most, and the encroachment on farmland and woodland is obvious. Under the ECS, the area of construction land increases relatively little, and the expansion mode is obviously different, mainly because the existing construction land has expanded slowly. Farmland and ecological protection policies limit the arbitrary expansion of construction land and play a certain role in protecting farmlands and woodlands. Under the CDS, except for the increase in construction land and water body areas, all other land types decrease, with the construction land area increasing the most, and woodland and farmland decreasing the most (Fig. 8).

The farmland area decreases under NDS and CDS (−7956.54 hm^2 and −12,133.53 hm^2, respectively) and decreases the most under CDS (−0.39%); however, it increases under ECS (+841.68 hm^2). The area of woodland decreases under all three scenarios, with reductions exceeding 1% under NDS and CDS, but this reduction is somewhat mitigated under the ECS scenario (−0.4%). The areas of water and construction land expand, with those of construction land expanding significantly. Under the CDS, construction land expanded the most, increasing by 32,151.06 hm^2, a 1.05% increase. However, it only increased by 5,012.73 hm^2 (+0.16%) in the ECS.

2030 CS

In 2030, the total CS values under the NDS, ECS and CDS scenarios are 653.46 × 10^6 t, 656.67 × 10^6 t, and 652.79 × 10^6 t, respectively. CS high-value areas are still widely distributed, with concentrations in the western and central forested areas, whereas low-value CS areas are concentrated in the southern main urban area and the southwest. These low-value areas continue to expand beyond the 2020 baseline, concentrating in areas of construction land and expanding water bodies (Fig. 9a–c). Among them, under the CDS and NDS, the CS of Zunyi is reduced by 5.57 × 10^6 t and 4.89 × 10^6 t, respectively, compared with that in 2020, with large decreases (0.85% and 0.74%, respectively). Under the ECS, the downward trend is significantly mitigated, with a decrease of only 1.68 × 10^6 t (0.26%) (Fig. 9d). Analyses of the spatial-temporal changes in CS from 2020 to 2030 show that, in general, the area of CS reduction is significantly larger than the area of CS increase under the three scenarios in Zunyi. The increased area is scattered and dotted throughout the whole region, and the decreased area is mainly in the southern and southwestern regions.

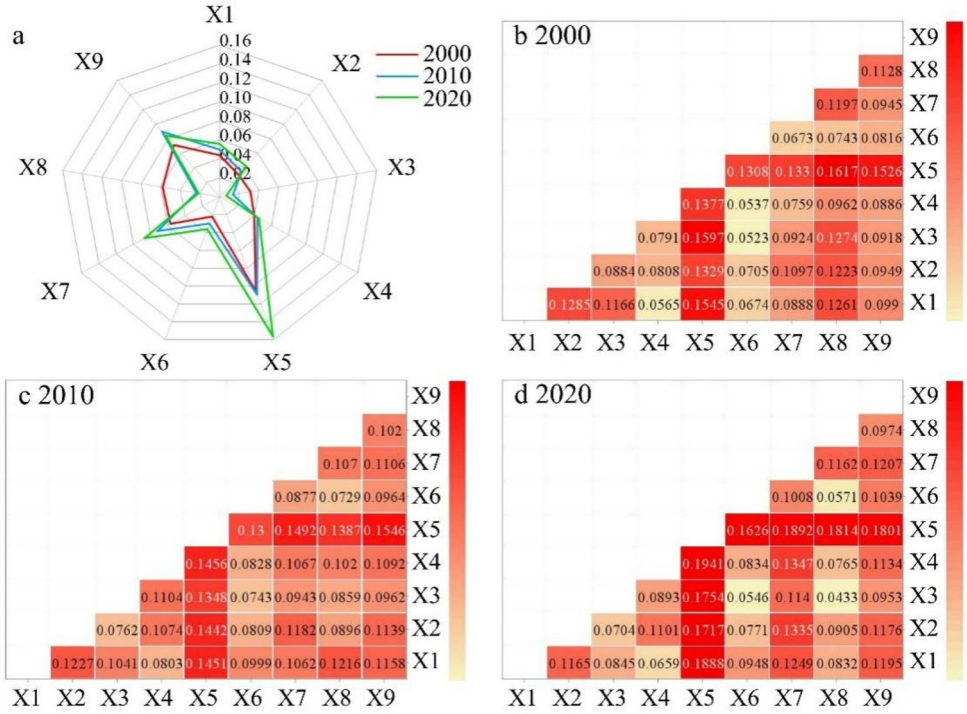

Fig. 7. (**a**) The q value of a single driver. (**b**,**c**,**d**) Explanatory power q value of the CS driven by two factors in Zunyi city (created by OriginLab Origin2021, https://www.originlab.com/).

The analysis of CS changes caused by land use changes reveals that under NDS, a reduction in farmland area leads to a loss of 1.22 × 10^6 t of CS, whereas a reduction in woodland area leads to a loss of 8.25 × 10^6 t of CS. Together, these two factors account for 1.94 times the total CS loss in this scenario, whereas the expansion of construction land leads to an increase of only 2.64 × 10^6 t of CS. Under the ECS, the increase in farmland results in an increase of 0.13 × 10^6 t of CS, and the loss of CS caused by woodland reduction is effectively controlled, leading to a CS reduction of only 3.08 × 10^6 t. Under the CDS, the significant reductions in woodland and farmland areas result in losses of 1.87 × 10^6 t and 9.07 × 10^6 t, respectively, whereas the large-scale expansion of construction land contributes to a CS increase of only 3.49 × 10^6 t. This situation shows that the effective control of woodland and farmland in the ECS weakens the trend of CS reduction. Owing to the high carbon density of woodlands, reasonable control of woodland transfer is the key to protecting ecosystem CS.

Discussion

Response of CS to land use change

Changes in land use types can alter the structure of ecosystems, leading to variations in soil carbon sequestration and vegetation carbon fixation capacity, which in turn cause changes in regional CS[42,43]. In this study, woodlands account for more than 62% of the area and are widely distributed, so the average values of both the total CS and the unit area in this region are high. Although the CS in the past 20 years tended to stabilize overall, it first tended to increase but then tended to decrease, similar to the change in forestland, which was consistent with the results of Yang et al. and Fu et al.[18,44]. From 2000 to 2010, the implementation of national policies such as returning farmland to forest and the construction of a nature protected area system enabled the woodland in Zunyi to be effectively protected and further expanded[45]. The transfer of farmland and grassland to woodland resulted in a net increase of 2.67 × 10^6 t CS, which was the main contributor to the increase in CS during this stage, which is consistent with the conclusion of Wu et al.[46]. From 2010 to 2020, the economy of Zunyi was effectively promoted. The urban expansion in southern China, the urbanization of counties and towns, and the rapid expansion of the wine-making scale of Renhuai in the southwest led to land use changes in this stage, which manifested as a reduction in farmland and woodland and an increase in construction land and water, resulting in the loss of CS[47–49].

Driving factors of CS

The OPGD model optimizes the discretization process of continuous variables and improves the accuracy of the detection results. Some studies have shown that there are differences in the q values detected by driving factors at different analysis scales[37,50]. Some studies choose the administrative region as the unit for driver factor analysis, whereas we choose to randomly select sampling points for analysis at a scale of 2 km within the research region. This may be the reason why the detection of driving factors generally results in lower values. The results indicate that both natural factors and socioeconomic factors have important impacts on the spatial distribution pattern of CS[51]. However, unlike previous studies[44], our study results show that the NDVI has a more significant impact.

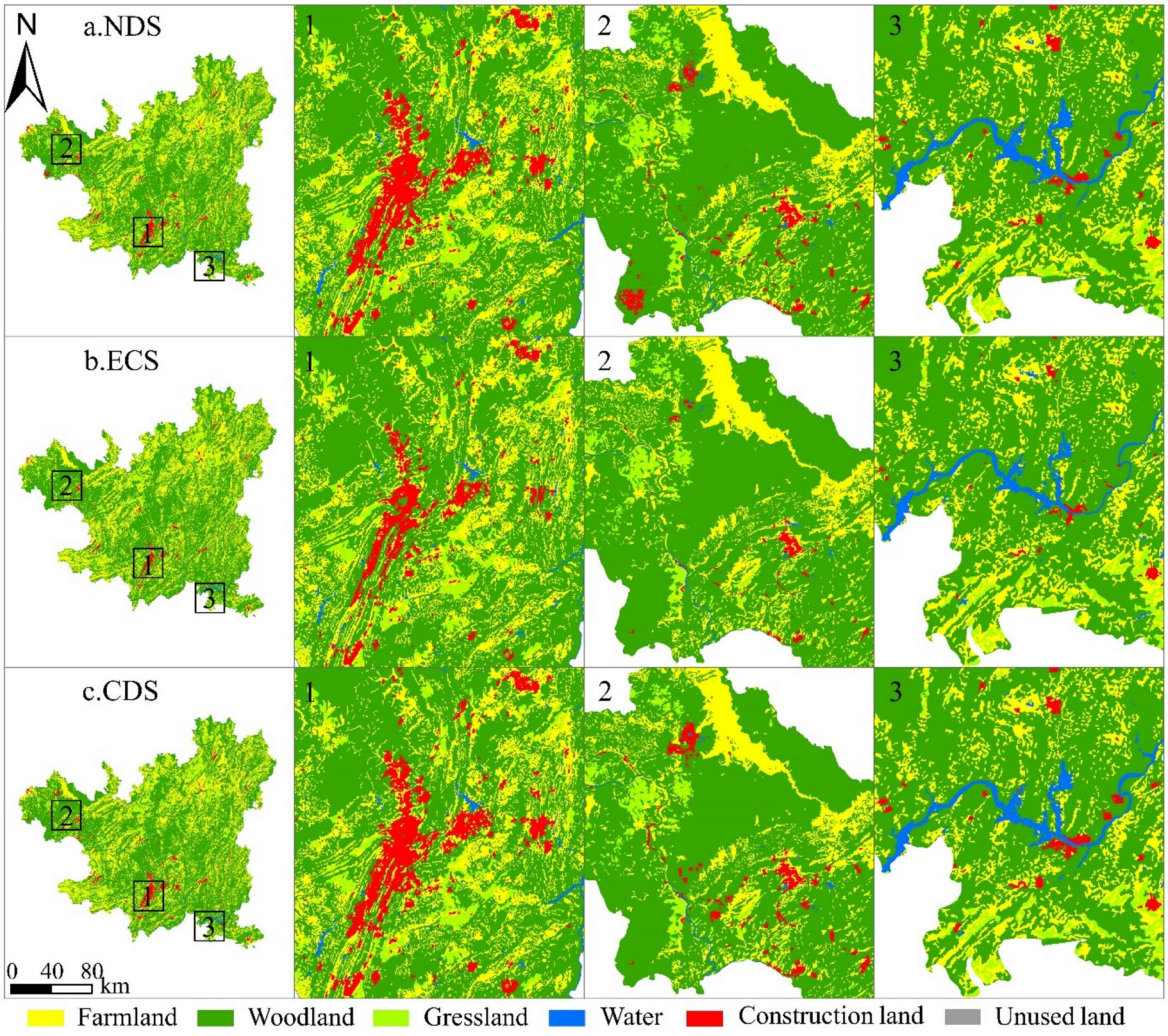

Fig. 8. The land use patterns of Zunyi in 2030 under multiple scenarios (created by ArcGIS 10.8, http://www.esri.com/).

The NDVI reflects vegetation cover and serves as a crucial indicator for quantifying vegetation growth conditions and the overall ecological environment. In Zunyi, many large natural forests with high vegetation coverage exist. Therefore, the NDVI value is relatively high, which directly affects the spatial pattern of CS. Additionally, research has shown that socioeconomic drivers such as the human footprint and population density significantly affect the CS. The 2021 Seventh National Population Census Report indicates that Zunyi city's population has increased by 479,593 people over the past 10 years (a growth rate of 7.83%)[52], and the urbanization process and population growth have led to an increase in the scale of central urban construction land and population density, thereby resulting in a decrease in CS. The human footprint index is a comprehensive indicator that reflects the pressure of human activities in a region, and it covers a variety of variables, such as buildings, the population, and roads[53]. Therefore, as Zunyi's economic development and human activities increase, the impact of the human footprint on the CS of the region continues to rise.

CS in future scenarios

Owing to the effective implementation of a series of ecological protection policies, such as the National Grain for Green Program and the Natural Forest Protection Project, the total CS of Zunyi remained relatively stable from 2000 to 2020[54]. During this era of sustainable economic development, we should focus on reasonably controlling the loss of CS. Some studies have shown that both farmland and woodland have strong carbon sequestration capacities because crops growing on the surface absorb carbon through photosynthesis; furthermore, soil has the ability to store carbon[17,55]. Therefore, enhancing the protection and utilization of farmland can help stabilize CS in urban areas and mitigate its decline[27,43]. Therefore, in this study, an ECS for the simultaneous protection of ecology and farmland was established[56]. Guided by the relevant opinions on overall national land space planning, this study aimed to limit the conversion of land types within nature reserves while reducing the probability of farmland and woodland conversion to other land types. This approach effectively curbs the

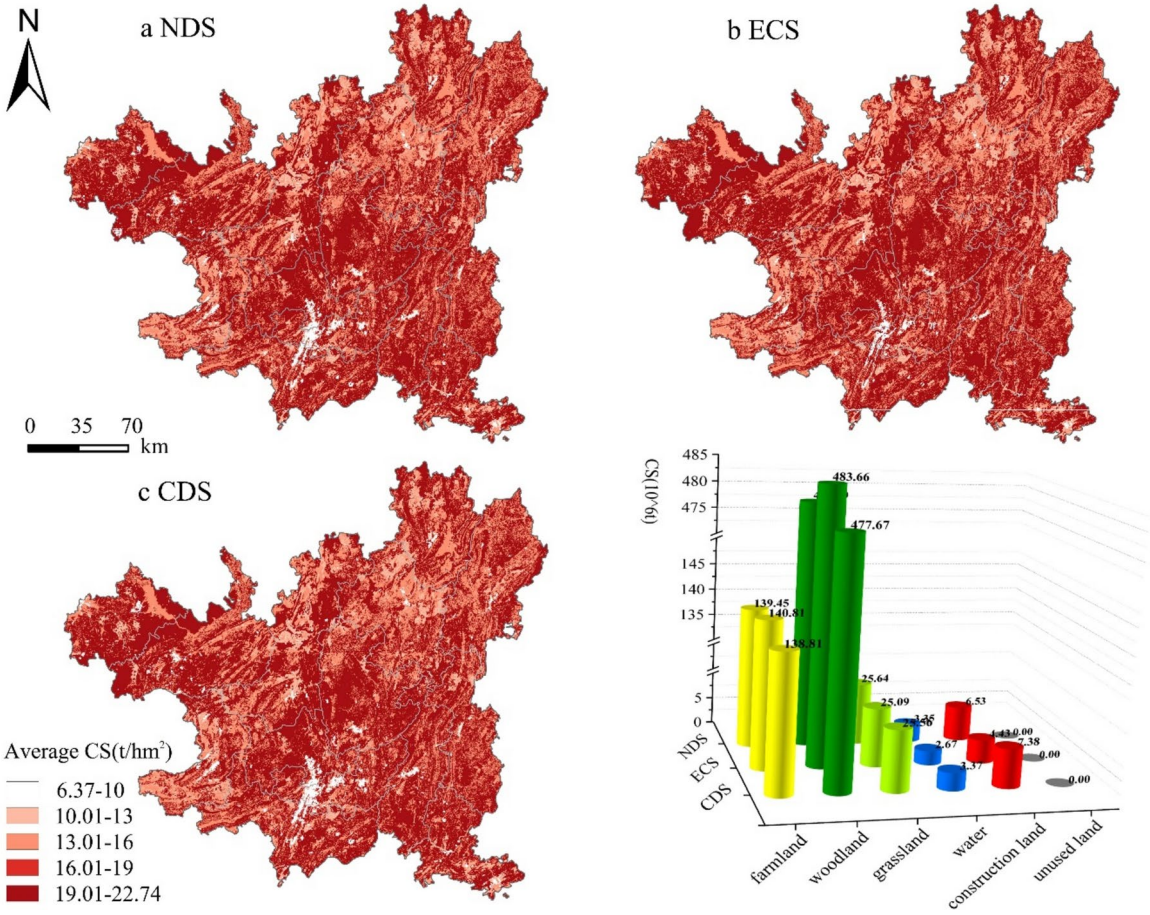

Fig. 9. (**a**,**b**,**c**) The land use patterns in 2030 under multiple scenarios. d. CS contributions by land use type under multiple scenarios (created by ArcGIS 10.8, http://www.esri.com/).

continuous reduction in woodlands and farmlands under the NDS scenario. At the same time, construction land effectively expanded on its original basis, contributing to the region's low-carbon sustainable development.

Limitations and prospects

First, although this study considered the influence of natural and socioeconomic factors on land use changes when the PLUS model was used for simulation, deviations still exist in the simulation results. For example, a comparison between 2020 simulation data and actual land use data revealed that the expansion of construction land exceeded expectations. Therefore, future simulation processes should fully consider the impacts of economic and regional policies to improve the accuracy of land use simulations. Second, only the carbon density of six land use types was considered in the evaluation of CS, and the differences in carbon density caused by different vegetation types were ignored[57]. The carbon pool data were corrected based on previous studies of carbon density in the region, introducing certain inaccuracies. In addition, this study only considers three scenarios. In particular, under the ECS, we have accounted for the importance of China's "Three Red Lines" policy in land use planning[4]. However, unfortunately, owing to data confidentiality, we were unable to obtain and apply this information in our simulation predictions. In the future, scenarios such as climate change should be considered to simulate future CS comprehensively from multiple perspectives[58,59].

Conclusions

In this study, we designed an integrated framework by combining the PLUS-InVEST-OPGD model, completing multi-scenario predictions of CS driven by multiple natural and socioeconomic factors. The final conclusions are as follows:

(1) Woodland and farmland are the main land use types in Zunyi. From 2000 to 2020, the land use transferred in Zunyi was 204,073.02 hm^2, which is reflected mainly in the mutual conversion among woodland, farmland, and grassland and by their conversion to construction land and water.
(2) The total CS of Zunyi is high and exhibits spatial clustering effects, with swoodland and farmland contributing more than 90% of the total CS. The total CS in Zunyi from 2000 to 2020 fluctuated, with an initial increase followed by a decrease, with land use changes significantly impacting this trend. In particular, the

transfer of woodland, farmland and grassland to construction land and water was the main source of CS loss.

(3) Both natural and socioeconomic factors have significant impacts on the spatial distribution of CS. The NDVI is the main driving factor (q > 10%), and its synergistic effects with population density and GDP exhibit a nonlinear enhancement on the CS. The impacts of the human footprint index and population density continuously increased.

(4) In 2030, the CS of Zunyi still shows a decreasing trend under the NDS, ECS and CDS. Under the ECS, the CS is the highest, with a reduction of only 1.68 × 10^6 t compared with that in 2020 (− 0.26%). The effective control of woodland and farmland in the ECS weakens the trend of CS reduction.

Data availability

The datasets used and/or analysed during the study available from the corresponding author on reasonable request.

Received: 11 June 2024; Accepted: 26 November 2024
Published online: 02 January 2025

References

1. Hong, C. et al. Global and regional drivers of land-use emissions in 1961–2017. *Nature* **589**, 554–561. https://doi.org/10.1038/s41586-020-03138-y (2021).
2. Cai, Z. et al. Assessment of eco-environmental quality changes and spatial heterogeneity in the Yellow River Delta based on the remote sensing ecological index and geo-detector model. *Ecol. Inf.* **77**, 102203. https://doi.org/10.1016/j.ecoinf.2023.102203 (2023).
3. Zhang, Z. et al. Simulation of temporal and spatial changes in ecosystem carbon storage in Funiu mountains based on InVEST model. *Environ. Sci.* **45**, 2332–2341. https://doi.org/10.13227/j.hjkx.202306203 (2024).
4. Liu, J. et al. How much carbon storage will loss in a desertification area? Multiple policy scenario analysis from Gansu Province. *Sci. Total Environ.* https://doi.org/10.1016/j.scitotenv.2023.169668 (2024).
5. Ning, J., Liu, J., Kuang, W., Xu, X. & Ning, J. Spatiotemporal patterns and characteristics of land-use change in China during 2010–2015. *J. Geograph. Sci.* **28**, 547–562. https://doi.org/10.1007/s11442-018-1490-0 (2018).
6. Zhao, X., Ma, X., Chen, B., Shang, Y. & Song, M. Challenges toward carbon neutrality in China: Strategies and countermeasures. *Resources Conserv. Recycling* **176**, 105959. https://doi.org/10.1016/j.resconrec.2021.105959 (2022).
7. Zhao, Y. et al. Is cooperative green innovation better for carbon reduction? Evidence from China. *J. Clean. Prod.* **394**, 136400. https://doi.org/10.1016/j.jclepro.2023.136400 (2023).
8. Zhong, Z. et al. Role of CO2 geological storage in China's pledge to carbon peak by 2030 and carbon neutrality by 2060. *Energy* **272**, 127165. https://doi.org/10.1016/j.energy.2023.127165 (2023).
9. Tang, R. et al. Air quality and health co-benefits of China's carbon dioxide emissions peaking before 2030. *Nat. Commun.* **13**, 1008. https://doi.org/10.1038/s41467-022-28672-3 (2022).
10. Bhagabati, N. K. et al. Ecosystem services reinforce Sumatran tiger conservation in land use plans. *Biol. Conserv.* **169**, 147–156. https://doi.org/10.1016/j.biocon.2013.11.010 (2014).
11. Wei, Q. et al. Temporal and spatial variation analysis of habitat quality on the PLUS-InVEST model for Ebinur Lake Basin, China. *Ecol. Indic.* **145**, 109632. https://doi.org/10.1016/j.ecolind.2022.109632 (2022).
12. Anley, M. A. & Minale, A. S. Modeling the impact of land use land cover change on the estimation of soil loss and sediment export using InVEST model at the Rib watershed of Upper Blue Nile Basin, Ethiopia. *Remote Sens. Appl. Soc. Environ.* **34**, 101177. https://doi.org/10.1016/j.rsase.2024.101177 (2024).
13. Ebi, K. L. et al. A new scenario framework for climate change research: Background, process, and future directions. *Clim. Change* **122**, 363–372. https://doi.org/10.1007/s10584-013-0912-3 (2014).
14. Sun, S. & Shi, Q. Global spatio-temporal assessment of changes in multiple ecosystem services under four IPCC SRES land-use scenarios. *Earth's Future* **8**, e2020EF001668. https://doi.org/10.1029/2020EF001668 (2020).
15. Zhang, H. et al. Comparing simulated atmospheric carbon dioxide concentration with GOSAT retrievals. *Sci. Bull.* **60**, 380–386. https://doi.org/10.1007/s11434-014-0676-9 (2015).
16. Wu, X. et al. Spatio-temporal evolution characteristics and simulation prediction of carbon storage: A case study in Sanjiangyuan Area, China. *Ecol. Inf.* **80**, 102485. https://doi.org/10.1016/j.ecoinf.2024.102485 (2024).
17. Jiang, W., Deng, Y., Tang, Z., Lei, X. & Chen, Z. Modelling the potential impacts of urban ecosystem changes on carbon storage under different scenarios by linking the CLUE-S and the InVEST models. *Ecol. Model.* **345**, 30–40. https://doi.org/10.1016/j.ecolmodel.2016.12.002 (2017).
18. Qiao, X. et al. Assessing current and future soil erosion under changing land use based on InVEST and FLUS models in the Yihe River Basin, North China. *Int. Soil Water Conserv. Res.* **12**, 298–312. https://doi.org/10.1016/j.iswcr.2023.07.001 (2024).
19. Wu, W. et al. Simulation and attribution analysis of terrestrial ecosystem carbon storage of Hainan Island from 2015 to 2050. *Sci. Total Environ.* **917**, 170348. https://doi.org/10.1016/j.scitotenv.2024.170348 (2024).
20. Feng, Y. et al. Modeling changes in China's 2000–2030 carbon stock caused by land use change. *J. Clean. Prod.* **252**, 119659. https://doi.org/10.1016/j.jclepro.2019.119659 (2020).
21. Xu, L. et al. Forecasting urban land use change based on cellular automata and the PLUS model. *Land* **11**, 652. https://doi.org/10.3390/land11050652 (2022).
22. Liang, X. et al. Understanding the drivers of sustainable land expansion using a patch-generating land use simulation (PLUS) model: A case study in Wuhan, China. *Comput. Environ. Urban Syst.* **85**, 101569. https://doi.org/10.1016/j.compenvurbsys.2020.101569 (2021).
23. Guo, B., Zang, W. & Luo, W. Spatial-temporal shifts of ecological vulnerability of Karst Mountain ecosystem-impacts of global change and anthropogenic interference. *Sci. Total Environ.* **741**, 140256. https://doi.org/10.1016/j.scitotenv.2020.140256 (2020).
24. Hu, Z. et al. Changes in ecosystem service values in karst areas of China. *Agric. Ecosyst. Environ.* **301**, 107026. https://doi.org/10.1016/j.agee.2020.107026 (2020).
25. Wang, R., An, Y., Wang, P. & Ma, L. Study on biodiversity conservation hotspots in Guizhou. *Res. Soil Water Conserv.* **21**, 6. https://doi.org/10.13869/j.cnki.rswc.2014.06.031 (2014).
26. Fan, H., Wang, X. J., Yang, Z. H., Wang, C. & Zhang, M. M. Spatial distribution characteristics and influencing factors of 4 main kind of protected areas in Zunyi City, Guizhou Province. *J. Ecol. Rural Environ.* **36**, 334–341. https://doi.org/10.19741/j.issn.1673-4831.2019.0902 (2020).
27. Zheng, H. & Zheng, H. Assessment and prediction of carbon storage based on land use/land cover dynamics in the coastal area of Shandong Province. *Ecol. Indic.* **153**, 110474. https://doi.org/10.1016/j.ecolind.2023.110474 (2023).

28. Chuai, X. et al. Land use structure optimization based on carbon storage in several regional terrestrial ecosystems across China. *Environ. Sci. Policy* **25**, 50–61. https://doi.org/10.1016/j.envsci.2012.05.005 (2013).
29. Li, M., Du, M. & Yu, L. Carbon storage and density of forest vegetation and its spatial distribution pattern in Guizhou Province. *J. Northwest For. Univ.* **31**, 48–54. https://doi.org/10.3969/j.issn.1001-7461.2016.01.09 (2016).
30. Jing, X. Research on the measurement and valuation of ecosystem services in Guizhou Province based on InVEST model. https://doi.org/10.27242/d.cnki.gnjlu.2021.000257 (2022).
31. Hu, S., Zhang, X. & Guan, D. Analysis on carbon storage change of construction land expansion in chongqing based on InVEST model. *Res. Soil Water. Conserv.* **25**, 323–331. https://doi.org/10.13869/j.cnki.rswc.2018.03.046 (2018).
32. Chen, D. et al. Analysis of carbon stock evolution and its vulnerability characteristics based on land use change in Guizhou. *Bull. Soil Water Conserv.* **43**, 301–309. https://doi.org/10.13961/j.cnki.stbctb.20230216.002 (2023).
33. Alam, S. A., Starr, M. & Clark, B. J. F. Tree biomass and soil organic carbon densities across the Sudanese woodland savannah: A regional carbon sequestration study. *J. Arid Environ.* **89**, 67–76. https://doi.org/10.1016/j.jaridenv.2012.10.002 (2013).
34. Liu, X. et al. A future land use simulation model (FLUS) for simulating multiple land use scenarios by coupling human and natural effects. *Landsc. Urban Plan.* **168**, 94–116. https://doi.org/10.1016/j.landurbplan.2017.09.019 (2017).
35. Yan, Z. et al. Spatial and temporal variation of NDVI and its driving factors based on geographical detector: A case study of Guanzhong plain urban agglomeration. *Remote Sens. Appl. Soc. Environ.* **32**, 101030. https://doi.org/10.1016/j.rsase.2023.101030 (2023).
36. Jiang, R. et al. Factors influencing the adoption of renewable energy in the U.S. residential sector: An optimal parameters-based geographical detector approach. *Renew. Energy* **201**, 450–461. https://doi.org/10.1016/j.renene.2022.09.084 (2022).
37. Zhao, X., Tan, S., Li, Y., Wu, H. & Wu, R. Quantitative analysis of fractional vegetation cover in southern Sichuan urban agglomeration using optimal parameter geographic detector model, China. *Ecol. Indic.* **158**, 111529. https://doi.org/10.1016/j.ecolind.2023.111529 (2024).
38. Zhu, X., Pan, J. & Wu, X. Impact of agricultural irrigation and resettlement practices on carbon storage in arid inland river basins: A case study of the Shule river basin. *Heliyon* **10**, e25305. https://doi.org/10.1016/j.heliyon.2024.e25305 (2024).
39. Zheng, H. & Li, H. Spatial–temporal evolution characteristics of land use and habitat quality in Shandong Province, China. *Sci. Rep.* **12**, 15422. https://doi.org/10.1038/s41598-022-19493-x (2022).
40. Xie, B. & Zhang, M. Spatio-temporal evolution and driving forces of habitat quality in Guizhou Province. *Sci. Rep.* **13**, 6908. https://doi.org/10.1038/s41598-023-33903-8 (2023).
41. Fan, L. et al. Scenario simulation of land use change and carbon storage response in Henan Province, China: 1990–2050. *Ecol. Indic.* **154**, 110660. https://doi.org/10.1016/j.ecolind.2023.110660 (2023).
42. Yakir, D. Large rise in carbon uptake by land plants. *Nature* **544**, 39–40. https://doi.org/10.1038/544039a (2017).
43. Bullock, E. L. & Woodcock, C. E. Carbon loss and removal due to forest disturbance and regeneration in the Amazon. *Sci. Total Environ.* **764**, 142839. https://doi.org/10.1016/j.scitotenv.2020.142839 (2021).
44. Fu, K., Chen, L., Yu, X. & Jia, G. How has carbon storage changed in the Yili-Tianshan region over the past three decades and into the future? What has driven it to change?. *Sci. Total Environ.* **945**, 174005. https://doi.org/10.1016/j.scitotenv.2024.174005 (2024).
45. Liang, Y., Hashimoto, S. & Liu, L. Integrated assessment of land-use/land-cover dynamics on carbon storage services in the Loess Plateau of China from 1995 to 2050. *Ecol. Indic.* **120**, 106939. https://doi.org/10.1016/j.ecolind.2020.106939 (2021).
46. Chang, X., Xing, Y., Wang, J., Yang, H. & Gong, W. Effects of land use and cover change (LUCC) on terrestrial carbon stocks in China between 2000 and 2018. *Resources Conserv. Recycling* **182**, 106333. https://doi.org/10.1016/j.resconrec.2022.106333 (2022).
47. Xiang, S. et al. Response and multi-scenario prediction of carbon storage to land use/cover change in the main urban area of Chongqing, China. *Ecol. Indic.* **142**, 109205. https://doi.org/10.1016/j.ecolind.2022.109205 (2022).
48. Wei, Y. & Chen, Q. Eco-environmental effects and prediction of land use transition for Zunyi City under background of carbon peaking. *Bull. Soil Water Conserv.* **43**, 388–398. https://doi.org/10.13961/j.cnki.stbctb.20221207.003 (2023).
49. Li, Y. & Luo, H. F. Carbon storage change of construction land expansion in central Guizhou's Karst Region based on InVEST model. *J. Northwest For. Univ.* **39**, 185–192 (2024).
50. Chen, S. et al. Synergy level of pollution and carbon reduction in the Yangtze River Economic Belt: Spatial-temporal evolution characteristics and driving factors. *Sustain. Cities Soc.* **98**, 104859. https://doi.org/10.1016/j.scs.2023.104859 (2023).
51. Li, Y. & Geng, H. Spatiotemporal trends in ecosystem carbon stock evolution and quantitative attribution in a karst watershed in southwest China. *Ecol. Indic.* **153**, 110429. https://doi.org/10.1016/j.ecolind.2023.110429 (2023).
52. Dong, Y., Ge, J., Liu, H. & Li, S. A study on the spatial distribution characteristics and influencing factors of floating population—based on the data of the 7th national population census. *J. Green Sci. Technol.* **25**, 193–198. https://doi.org/10.16663/j.cnki.lskj.2023.17.036 (2023).
53. Mu, H. et al. A global record of annual terrestrial Human Footprint dataset from 2000 to 2018. *Sci. Data* **9**, 176. https://doi.org/10.1038/s41597-022-01284-8 (2022).
54. Wu, Q., Wang, L., Wang, T., Ruan, Z. & Du, P. Spatial–temporal evolution analysis of multi-scenario land use and carbon storage based on PLUS-InVEST model: A case study in Dalian, China. *Ecol. Indic.* **166**, 112448. https://doi.org/10.1016/j.ecolind.2024.112448 (2024).
55. Armenteras, D., Murcia, U., González, T. M., Barón, O. J. & Arias, J. E. Scenarios of land use and land cover change for NW Amazonia: Impact on forest intactness. *Global Ecol. Conserv.* **17**, e00567. https://doi.org/10.1016/j.gecco.2019.e00567 (2019).
56. Tang, L., Ke, X., Zhou, T., Zheng, W. & Wang, L. Impacts of cropland expansion on carbon storage: A case study in Hubei, China. *J. Environ. Manag.* **265**, 110515. https://doi.org/10.1016/j.jenvman.2020.110515 (2020).
57. Wang, Z. et al. Dynamic simulation of land use change and assessment of carbon storage based on climate change scenarios at the city level: A case study of Bortala, China. *Ecol. Indic.* **134**, 108499. https://doi.org/10.1016/j.ecolind.2021.108499 (2022).
58. Zhao, M. et al. Assessing the effects of ecological engineering on carbon storage by linking the CA-Markov and InVEST models. *Ecol. Indic.* **98**, 29–38. https://doi.org/10.1016/j.ecolind.2018.10.052 (2019).
59. Wang, H., Wu, L., Yue, Y., Jin, Y. & Zhang, B. Impacts of climate and land use change on terrestrial carbon storage: A multi-scenario case study in the Yellow River Basin (1992–2050). *Sci. Total Environ.* **930**, 172557. https://doi.org/10.1016/j.scitotenv.2024.172557 (2024).

Acknowledgements

This work was supported by the National Natural Science Foundation of China (Grant Number 32260331). We would like to thank the editors and the reviewers for their constructive comments and suggestions to improve our manuscript.

Author contributions

M.Z. designed and directed the study. Material preparation, data analysis were performed by Y.L., X.M. and L.Y.. The manuscript was written by Y.L.. M.Z. reviewed and edited the manuscript. All authors have read and approved the version of the manuscript to be published.

Competing interests
The authors declare no competing interests.

Additional information
Supplementary Information The online version contains supplementary material available at https://doi.org/10.1038/s41598-024-81444-5.

Correspondence and requests for materials should be addressed to M.Z.

Reprints and permissions information is available at www.nature.com/reprints.

Publisher's note Springer Nature remains neutral with regard to jurisdictional claims in published maps and institutional affiliations.